Phosphorus

International Edition: DOI: 10.1002/anie.201611740
German Edition: DOI: 10.1002/ange.201611740

Assembly of Ring-Shaped Phosphorus within Carbon Nanotube Nanoreactors

Jinying Zhang, Dan Zhao, Dingbin Xiao, Chuansheng Ma, Hongchu Du, Xin Li, Lihui Zhang, Jialiang Huang, Hongyang Huang, Chun-Lin Jia,* David Tománek,* and Chunming Niu*

Abstract: *A phosphorus allotrope that has not been observed so far, ring-shaped phosphorus consisting of alternate P_8 and P_2 structural units, has been assembled inside multi-walled carbon nanotube nanoreactors with inner diameters of 5–8 nm by a chemical vapor transport and reaction of red phosphorus at 500 °C. The ring-shaped nanostructures with surrounding graphene walls are stable under ambient conditions. The nanostructures were characterized by high-resolution transmission electron microscopy, scanning transmission electron microscopy, energy-dispersive X-ray spectroscopy, Raman scattering, attenuated total reflectance Fourier transform infrared spectroscopy, and X-ray photoelectron spectroscopy.*

Two-dimensional (2D) black phosphorus, phosphorene, has attracted lots of attention owing to its intrinsic electronic properties.[1–4] However, phosphorene has been found to degrade under ambient conditions[5] and needs to be protected by an inert atmosphere[3] or specific molecules[6,7] owing to its reactivity caused by lone electron pairs. Several other interesting phosphorus allotropes have also been theoretically predicted.[8–11] Experimentally well-established is the white phosphorus allotrope, a molecular solid consisting of P_4 molecules. Other established allotropes that have been produced experimentally, include Hittorf phosphorus (violet phosphorus),[12] fibrous phosphorus,[13] blue phosphorus,[14] and black phosphorus,[3,15,16] as well as amorphous red phosphorus[17] (RP). Published theoretical predictions include a stable ring-shaped phosphorus (*r*-P) allotrope consisting of alternating P_8 and P_2 structural units with minimum stability reached for P_{80},[10] and coil structures.[11] Carbon nanotubes are effective as nanoreactors to synthesize and contain nanostructures.[18–27] Carbon nanotubes also serve as narrow and stable one-dimensional cages that protect the enclosed products from degradation under ambient conditions.

Herein, we report experimental evidence for the formation of *r*-P nanostructures, self-assembled inside a multi-walled carbon nanotube (MWCNT). The *r*-P nanostructures inside MWCNTs (*r*-P@MWCNTs) are stable under ambient conditions. The nanostructures have been characterized by high-resolution transmission electron microscopy (HRTEM), scanning transmission electron microscopy (STEM), STEM energy-dispersive X-ray spectroscopy (EDS), Raman scattering, attenuated total reflectance Fourier transform infrared spectroscopy (ATR-FTIR), and X-ray photoelectron spectroscopy (XPS).

MWCNTs functioning as nanoreactors were prepared by a CVD method to have less than 0.9 % catalyst[28] and purified according to a reported method.[29] The *r*-P@MWCNTs were prepared by a vapor-phase transportation and reaction method[19–21,30,31] at 500 °C using RP as precursor. At 500 °C, RP was sublimed and likely decomposed into different phosphorus clusters (PCs), which subsequently diffused into evacuated inner space of MWCNTs and self-assembled to form *r*-P nanostructures to give an encapsulation yield around 60 %.

The encapsulation of phosphorus into MWCNTs was confirmed by STEM and EDS analysis. As shown in Figure 1 a, the brighter image contrast in a high-angle annular dark-field (HAADF) image of the encapsulated molecules than the surrounding MWCNT suggests that heavier elements than carbon were encapsulated inside MWCNTs. The encapsulated molecules in MWCNTs were confirmed to be phosphorus by elemental maps of P and C (Figure 1 b–d). Two parallel CNTs are included in the image of Figure 1, which provides evidence for distinguishing a filled CNT by P (top CNT) from an empty one (bottom CNT).

The structure of the encapsulated phosphorus in CNT was investigated by the negative spherical aberration imaging (NCSI) technique.[32,33] In comparison with conventional bright-field HRTEM imaging under the conditions of underfocus combined with positive spherical aberration, where the atoms would appear black, the NCSI technique results in a higher contrast of image and higher signal intensity at atom positions. The high contrast and signal intensity show great advantage against the disturbance of noise and for measurement of atom positions at picometer precision. Figure 2 a shows a NCSI image recorded at 80 kV. In the image, atoms

[*] Dr. J. Zhang, D. Zhao, D. Xiao, X. Li, L. Zhang, J. Huang, H. Huang, Prof. C.-M. Niu
Center of Nanomaterials for Renewable Energy
State Key Laboratory of Electrical Insulation and Power Equipment
School of Electrical Engineering, Xi'an Jiaotong University
Xi'an, Shaanxi, 710049 (P.R. China)
E-mail: jinying.zhang@mail.xjtu.edu.cn
C. Ma, Prof. C. L. Jia
The School of Electronic and Information Engineering and State Key Laboratory for Mechanical Behaviour of Materials
Xi'an Jiaotong University
Xi'an, Shaanxi, 710049 (P.R. China)
E-mail: c.jia@mail.xjtu.edu.cn
Dr. H. Du, Prof. C. L. Jia
Ernst Ruska Centre for Microscopy and Spectroscopy with Electrons
Forschungszentrum Jülich, 52425 Jülich (Germany)
Prof. D. Tománek
Physics and Astronomy Department, Michigan State University
East Lansing, MI 48824-2320 (USA)
E-mail: tomanek@pa.msu.edu

Supporting information for this article can be found under: http://dx.doi.org/10.1002/anie.201611740.

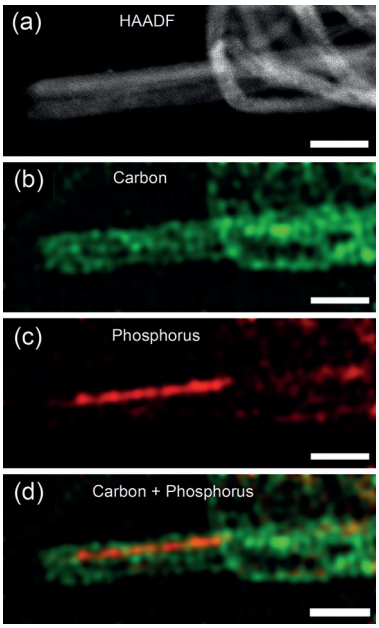

Figure 1. a) A representative high-angle annular dark-field (HAADF) image of *r*-P@MWCNTs. b)–d) The corresponding elemental maps of C, P and C + P of *r*-P@MWCNTs. Scale bar = 200 nm. FEI Titan G2 80–200 ChemiSTEM microscope, accelerating voltage: 80 kV.

and atomic planes (rings) appear bright against a dark background. Whereas the structure of the enclosing MWCNT is well-resolved and understood, the structure of elemental phosphorus filling the wide space inside may be significantly more complex than atomic arrangements previously observed in much narrower nanotubes.[34,35] The details of the image contrast in the region adjacent to the innermost wall appear consistent with an *r*-P structure with sp^3 hybridization inside the MWCNT, shown in Figure 2 b,c. The minimum stable ring is P_{80}, being $-13.3\ kJ\,mol^{-1}$ per atom more stable than the P_4 in terms of total energy. The ring structures become increasingly more stable until P_{200}.[10] A related theoretical study characterized the properties of a related structure consisting of helical coils (rather than stacked rings) with the same local atomic arrangement.[11] The shape and size of the *r*-P subunits can also be recognized, which fit to a P_8 structure as shown by a projected P_8 structure model superimposed on the NCSI image (Figure 2 a, inset). Image simulation was performed on the basis of *r*-P@MWCNT models shown in Figure 2 b using a single layer ring of *r*-P, with the space inside the rings assumed to be vacant. The simulation result is consistent with the experimental image (left part of the image). We notice that in the right part of the image, the feature of *r*-P can be recognized in the lower part only, while in the upper part this feature disappears. This can be understood as the result of half rings or damage from electron irradiation. Figure 2 b shows the model of the *r*-P@MWCNT in atomic detail. The phosphorus ring is comprised of 230 atoms (Figure 2 c) and has a diameter of 5.30 nm with inter-ring distance of 6.4 Å inside a MWCNT with inner diameter of 5.90 nm. Furthermore, multilayer *r*-P in MWCNTs was also observed in our experiments (Supporting Information, Figure S1).

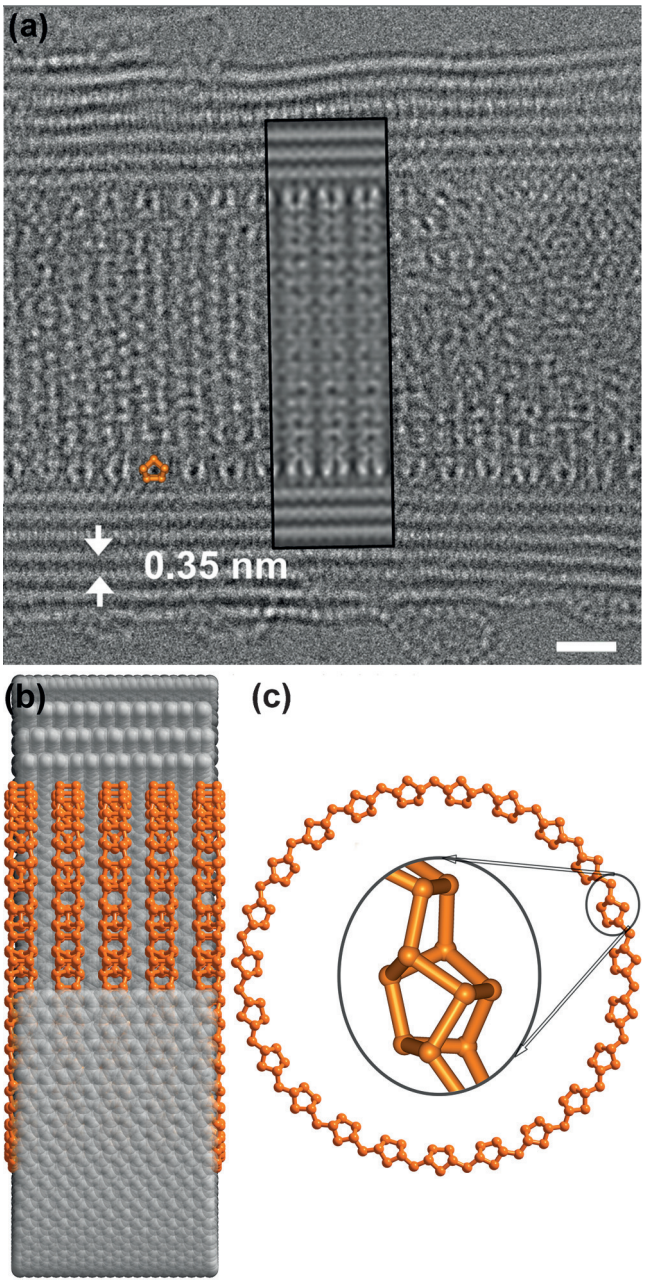

Figure 2. a) NCSI image of a *r*-P@MWCNT. Insets: simulation of the *r*-P@MWCNT (in black box) based on the structural model in (b) and structural model of P_8 (orange). Scale bar = 1 nm. FEI Titan^3 60–300 (PICO) microscope equipped with a spherical-chromatic aberration corrector, accelerating voltage: 80 kV. b) Structural model of *r*-P@MWCNTs, c) side view of *r*-P (inset shows the repeating units).

The *r*-P nanostructures were observed inside MWCNTs with inner diameters between 5 nm to 8 nm (Supporting Information, Figure S1). The HRTEM images of self-assembled *r*-P nanostructures in MWCNTs are distinguishable from recently reported phosphorus nanorods[36] and fibrous RP,[13] which have been observed by HRTEM as black lines in bulk structures. The two phosphorus nanorod structures of $-[-[P_8]P_4-]-$ and $-[-[P_{10}]P_2-]-$ were observed by HRTEM to be parallel lines with diameter of 3.3 Å (line distance of 5.0 Å,)

and 4.7 Å (line distance of 5.4 Å).[36] On the other hand, parallel strands with distance of 3.2 Å were observed from fibrous RP.[13]

The self-assembled *r*-P nanostructures inside MWCNTs are stable in air, since the lone pair electrons of phosphorus are passivated by the intact walls of carbon nanotubes (Supporting Information, Figure S1). The ends of self-assembled *r*-P nanostructures at the opening of MWCNTs are passivated by either an atomically thin layer of amorphous carbon, or by phosphorus or phosphorus oxides (Supporting Information, Figure S2). The space restriction imposed by MWCNTs limits volume expansion needed for further oxidation and oxygen diffusion when exposed to air. The HRTEM investigations further confirmed that carbon nanotubes are efficient Faraday tubes for phosphorus nanostructures.

The structures of *r*-P@MWCNTs were also characterized by ATR-FTIR, Raman scattering (Figure 3), and XPS. The as-decomposed PCs were not only assembled into the evacuated capsules of MWCNTs to form *r*-P nanostructures, but also condensed outside the MWCNTs as amorphous and crystalline RP during vapor-phase reactions (Supporting Information, Figure S3a). The amorphous phosphorus structures, formed on the external surfaces of MWCNTs, were oxidized immediately into phosphorus oxides when exposed to air. P–O vibrations at 1004 cm^{-1} and 1150 cm^{-1}, corresponding to phosphorus oxides,[37] are present in the ATR-FTIR spectra recorded under ambient conditions from an as-made *r*-P@MWCNT sample (Figure 3a, blue dotted line), and disappeared after washing with ethanol or CS_2 (Figure 3a, red dashed line) or gradient temperature cooling treatment (Figure 3a, black solid line). However, the crystalline RP on the external surfaces of MWCNTs is relatively stable, and still detectable by HRTEM (Supporting Information, Figure S3b) and Raman (Figure 3b, red dashed line) after washing with ethanol or CS_2, which was not observed from pristine MWCNTs (Figure 3b, green dotted line). The Raman features of phosphorus (300–600 cm^{-1}) are very weak compared to the G-band of MWCNTs under ambient conditions (Supporting Information, Figure S4a), which is hardly observed from quartz containers filled with Ar with both excitation wavelengths of 514 and 633 nm (Supporting Information, Figure S4b). The Raman features of phosphorus from *r*-P@MWCNTs are strongest with excitation laser power around 1 mW (633 nm) (Supporting Information, Figure S5, black). They can barely be observed at low or high power due to the low penetration and sublimation of phosphorus, respectively.

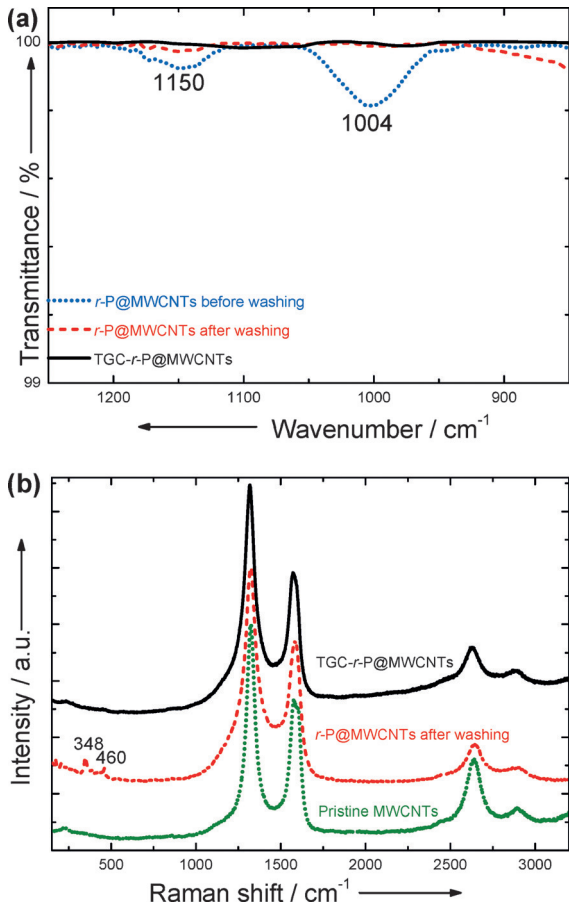

Figure 3. a) ATR-FTIR and b) Raman spectra of MWCNTs and *r*-P@MWCNTs at different stages under ambient conditions.

A gradient temperature cooling method was used to remove external phosphorus and obtain TGC-*r*-P@MWCNTs. Most of the external phosphorus has been removed from the *r*-P@MWCNTs to keep the encapsulation yield of more than 30% (Supporting Information, Figure S3c). However, no Raman features of phosphorus were detected from the TGC-*r*-P@MWCNTs sample using excitation lasers at either 514 or 633 nm (Supporting Information, Figure S6) with different laser powers. The G-band had sharpened after encapsulation of phosphorus (Figure 3b), indicating charge doping of the carbon nanotubes.[38] A blue-shift (+4 cm^{-1}) of the G-band was observed in *r*-P@MWCNTs with both external and internal phosphorus (Figure 3b, red dashed line) owing to hole doping[39] caused by external phosphorus oxides. However, a small red-shift (−2 cm^{-1}) of the G-band was observed from TGC-*r*-P@MWCNTs (Figure 3b, black solid line) in comparison to pristine MWCNTs (Figure 3b, green dotted line) owing to electron doping[40] of the lone electron pairs from phosphorus. This shift further confirmed the passivation effect of carbon walls on lone pair electrons of phosphorus. No P–P vibrations in the *r*-P nanostructures and small amount of external phosphorus were detected in the *r*-P@MWCNT sheets after gradient temperature treatment even when the scanning time was extended to 500 s and laser power increased to 7 mW.

XPS was also performed to understand the chemical bonding of the *r*-P structures (Figure 4). Argon ion beam etching (3 kV, 2.8 Å s^{-1}) was used to obtain a depth profile of P 2p spectra of *r*-P@MWCNT sample, since crystalline RP structures outside the nanotubes cannot be totally eliminated and the XPS is surface sensitive. No phosphorus oxides were detected by ATR-FTIR even with 4000 scans after washing by ethanol or CS_2 (Figure 3a, red dashed line), but could easily be detected in XPS. The XPS spectrum of *r*-P@MWCNT sample before etching (Figure 4, *r*-P@MWCNTs 0 s) was dominated by the surface oxides and external RP outside MWCNTs. The P 2p core-level binding energies are very

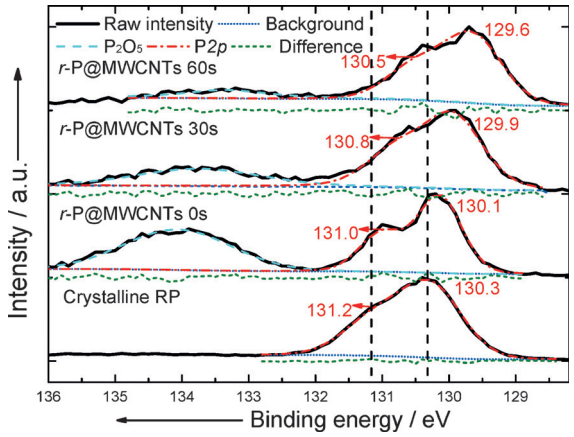

Figure 4. XPS depth profile of *r*-P@MWCNTs sample at various Ar^+ etching time (etching rate = 2.8 Å s^{-1}).

close to those of the RP precursor (Figure 4, crystalline RP). Phosphorus oxides were then gradually removed with increasing etching depth and became nearly undetectable after etching for 60 s (16.8 nm). The XPS spectrum then became dominated by the *r*-P structures inside carbon nanotubes instead of the crystalline RP outside MWCNTs. The P 2p core-level binding energies of *r*-P inside MWCNTs are smaller than those in bulk RP or external RP owing to the different structure and strain caused by the surrounding MWCNTs, analogous to the observation of sulfur inside carbon nanotubes.[34] Independent calculations[11] suggest the ring-like phosphorus structures to be direct-gap semiconductors with the gap exceeding 1.8 eV.

In summary, a previously unobserved phosphorus allotrope nanostructure has been self-assembled inside the evacuated MWCNTs. HRTEM image and structural simulation suggested that the observed nanostructure is *r*-P, which has been theoretically predicted to be stable but never experimentally observed. The *r*-P consists of alternate P_8 and P_2 structural units with variable ring diameters, observed inside the MWCNTs with inner diameters of 5–8 nm. A ring with a diameter of 5.30 nm, consisting of 23 P_8 and 23 P_2 units with a total of 230 P atoms, was observed inside a MWCNT with an inner diameter of 5.90 nm. The distance between neighboring rings is 6.4 Å. The surrounding graphitic walls of MWCNTs establish a nanoreactor for *r*-P structure formation and its protection against oxidation in air. A blue-shift of the G-band was observed from the sample containing both external and internal phosphorus, whereas a small red-shift was observed after removing most of the external phosphorus. The depth profile of P 2p XPS spectra of *r*-P@MWCNT shows that phosphorus oxides were distributed on the surfaces of the sample and could be etched away with an Ar ion beam. Observed P 2p core-level binding energies of *r*-P inside MWCNTs are smaller than external phosphorus.

Experimental Section

Degassed MWCNTs were sealed with extra red phosphorus (Aladdin, 99.999 % metals basis) under a vacuum of 10^{-5} Pa, heated at 500 °C for 48 h, and then cooled down in oven or under a temperature gradient condition (one end about 50–100 °C lower than the other end where the MWCNTs were present). XPS measurements were performed using a monochromatized Al Kα X-ray source (Thermo Scientific K-Alpha) at a base pressure of 10^{-9} Torr. The X-ray beam size was 400 μm × 600 μm and the argon ion etch crater was about 4 mm × 2 mm for depth profiles. The etching voltage was 3 kV with a etching rate of 2.8 Å s^{-1}. High-resolution transmission electron microscopy investigations were carried out at an acceleration voltage of 80 kV on an FEI Titan^3 60–300 (PICO) microscope equipped with a high-brightness field emission gun, a monochromator, and a C_S-C_C (spherical-chromatic aberration) achro-aplanat image corrector for the objective lens, providing an attainable resolution of 80 pm[41] and at 300 kV on an FEI Titan G2 microscope. Scanning transmission electron microscopy combined with energy dispersive X-ray (EDX) spectrum imaging was conducted at 80 kV on an FEI Titan G2 80–200 ChemiSTEM microscope equipped with a high-brightness Schottky field emission electron gun, a probe C_S corrector, and a Super-X EDX system, and also on a JEM-ARM200F microscope[42] with a probe C_S corrector. A nonlinear filtering algorithm was used for denoising of the elemental maps.[43]

Acknowledgements

We acknowledge useful discussions with Sumio Iijima, Dan Liu, Jie Guan, and Jingwei Jiang. This work has been supported by the National Natural Science Foundation of China (51302210, 51521065), Natural Science Foundation of Shaanxi Province (2015JQ5148), and by the Fundamental Research Funds for the Central Universities. D.T. was supported by the NSF/AFOSR EFRI 2-DARE grant number EFMA-1433459.

Conflict of interest

The authors declare no conflict of interest.

Keywords: allotropes · carbon nanotubes · nanoreactors · phosphorus · vapor-phase reactions

How to cite: *Angew. Chem. Int. Ed.* **2017**, *56*, 1850–1854
Angew. Chem. **2017**, *129*, 1876–1880

[1] H. Liu, A. T. Neal, Z. Zhu, Z. Luo, X. Xu, D. Tománek, P. D. Ye, *ACS Nano* **2014**, *8*, 4033.
[2] J. Guan, Z. Zhu, D. Tománek, *Phys. Rev. Lett.* **2014**, *113*, 046804.
[3] J. Kang, J. D. Wood, S. A. Wells, J. H. Lee, X. L. Liu, K. S. Chen, M. C. Hersam, *ACS Nano* **2015**, *9*, 3596.
[4] R. A. Doganov, E. C. T. O'Farrell, S. P. Koenig, Y. Yeo, A. Ziletti, A. Carvalho, D. K. Campbell, D. F. Coker, K. Watanabe, T. Taniguchi, A. H. Castro Neto, B. Ozyilmaz, *Nat. Commun.* **2015**, *6*, 6647.
[5] A. Castellanos-Gomez, L. Vicarelli, E. Prada, J. O. Island, K. L. Narasimha-Acharya, S. I. Blanter, D. J. Groenendijk, M. Buscema, G. A. Steele, J. V. Alvarez, H. W. Zandbergen, J. J. Palacios, H. S. J. van der Zant, *2D Mater.* **2014**, *1*, 025001.
[6] D. Hanlon, C. Backes, E. Doherty, C. S. Cucinotta, N. C. Berner, C. Boland, K. Lee, A. Harvey, P. Lynch, Z. Gholamvand, S. Zhang, K. Wang, G. Moynihan, A. Pokle, Q. M. Ramasse, N. McEvoy, W. J. Blau, J. Wang, G. Abellan, F. Hauke, A. Hirsch, S. Sanvito, D. D. O'Regan, G. S. Duesberg, V. Nicolosi, J. N. Coleman, *Nat. Commun.* **2015**, *6*, 8563.

[7] G. Abellán, V. Lloret, U. Mundloch, M. Marcia, C. Neiss, A. Goerling, M. Varela, F. Hauke, A. Hirsch, *Angew. Chem. Int. Ed.* **2016**, *55*, 14557; *Angew. Chem.* **2016**, *128*, 14777.
[8] J. Guan, Z. Zhu, D. Tománek, *Phys. Rev. Lett.* **2014**, *113*, 226801.
[9] Z. Zhu, D. Tománek, *Phys. Rev. Lett.* **2014**, *112*, 176802.
[10] A. J. Karttunen, M. Linnolahti, T. A. Pakkanen, *Chem. Eur. J.* **2007**, *13*, 5232.
[11] D. Liu, J. Guan, J. Jiang, D. Tománek, *Nano Lett.* **2016**, *16*, 7865.
[12] J. W. Hittorf, *Ann. Phys.* **1865**, *202*, 193.
[13] M. Ruck, D. Hoppe, B. Wahl, P. Simon, Y. K. Wang, G. Seifert, *Angew. Chem. Int. Ed.* **2005**, *44*, 7616; *Angew. Chem.* **2005**, *117*, 7788.
[14] J. L. Zhang, S. Zhao, C. Han, Z. Wang, S. Zhong, S. Sun, R. Guo, X. Zhou, C. D. Gu, K. D. Yuan, Z. Li, W. Chen, *Nano Lett.* **2016**, *16*, 4903.
[15] A. H. Woomer, T. W. Farnsworth, J. Hu, R. A. Wells, C. L. Donley, S. C. Warren, *ACS Nano* **2015**, *9*, 8869.
[16] P. Yasaei, B. Kumar, T. Foroozan, C. H. Wang, M. Asadi, D. Tuschel, J. E. Indacochea, R. F. Klie, A. Salehi-Khojin, *Adv. Mater.* **2015**, *27*, 1887.
[17] R. Hultgren, N. S. Gingrich, B. E. Warren, *J. Chem. Phys.* **1935**, *3*, 351.
[18] A. N. Khlobystov, *ACS Nano* **2011**, *5*, 9306.
[19] J. Zhang, Y. Miyata, R. Kitaura, H. Shinohara, *Nanoscale* **2011**, *3*, 4190.
[20] J. Zhang, Z. Zhu, Y. Feng, H. Ishiwata, Y. Miyata, R. Kitaura, J. E. P. Dahl, R. M. K. Carlson, N. A. Fokina, P. R. Schreiner, D. Tománek, H. Shinohara, *Angew. Chem. Int. Ed.* **2013**, *52*, 3717; *Angew. Chem.* **2013**, *125*, 3805.
[21] J. Zhang, Y. Feng, H. Ishiwata, Y. Miyata, R. Kitaura, J. E. P. Dahl, R. M. K. Carlson, H. Shinohara, D. Tománek, *ACS Nano* **2012**, *6*, 8674.
[22] A. Botos, J. Biskupek, T. W. Chamberlain, G. A. Rance, C. T. Stoppiello, J. Sloan, Z. Liu, K. Suenaga, U. Kaiser, A. N. Khlobystov, *J. Am. Chem. Soc.* **2016**, *138*, 8175.
[23] A. Chuvilin, E. Bichoutskaia, M. C. Gimenez-Lopez, T. W. Chamberlain, G. A. Rance, N. Kuganathan, J. Biskupek, U. Kaiser, A. N. Khlobystov, *Nat. Mater.* **2011**, *10*, 687.
[24] J. H. Warner, Y. Ito, M. H. Ruemmeli, T. Gemming, B. Buechner, H. Shinohara, G. A. D. Briggs, *Phys. Rev. Lett.* **2009**, *102*, 195504.
[25] D. A. Britz, A. N. Khlobystov, K. Porfyrakis, A. Ardavan, G. A. D. Briggs, *Chem. Commun.* **2005**, 37.
[26] L. Guan, K. Suenaga, S. Okubo, T. Okazaki, S. Lijima, *J. Am. Chem. Soc.* **2008**, *130*, 2162.
[27] L. H. Guan, K. Suenaga, S. Iijima, *Nano Lett.* **2008**, *8*, 459.
[28] X. Li, Z. Wang, J. Zhang, C. Xie, B. Li, R. Wang, J. Li, C. Niu, *Carbon* **2015**, *85*, 168.
[29] K. Kamalasanan, R. Gottardi, S. Tan, Y. Chen, B. Godugu, S. Rothstein, A. C. Balazs, A. Star, S. R. Little, *Angew. Chem. Int. Ed.* **2013**, *52*, 11308; *Angew. Chem.* **2013**, *125*, 11518.
[30] J. X. Xu, L. H. Guan, *RSC Adv.* **2013**, *3*, 5577.
[31] J. Zhang, F. Zhou, Y. Miyata, R. Kitaura, H. Su, H. Shinohara, *RSC Adv.* **2014**, *3*, 16954.
[32] C. L. Jia, M. Lentzen, K. Urban, *Science* **2003**, *299*, 870.
[33] C. L. Jia, L. Houben, A. Thust, J. Barthel, *Ultramicroscopy* **2010**, *110*, 500.
[34] T. Fujimori, A. Morelos-Gomez, Z. Zhu, H. Muramatsu, R. Futamura, K. Urita, M. Terrones, T. Hayashi, M. Endo, S. Y. Hong, Y. C. Choi, D. Tomanek, K. Kaneko, *Nat. Commun.* **2013**, *4*, 2162.
[35] T. Fujimori, R. B. dos Santos, T. Hayashi, M. Endo, K. Kaneko, D. Tomanek, *ACS Nano* **2013**, *7*, 5607.
[36] A. Pfitzner, M. F. Brau, J. Zweck, G. Brunklaus, H. Eckert, *Angew. Chem. Int. Ed.* **2004**, *43*, 4228; *Angew. Chem.* **2004**, *116*, 4324.
[37] K. Nakamoto, *Infrared and Raman Spectra Of Inorganic And Coordination Compounds Part A*, 6th ed., Wiley, Hoboken, **2009**, p. 177.
[38] A. C. Ferrari, *Solid State Commun.* **2007**, *143*, 47.
[39] A. Das, S. Pisana, B. Chakraborty, S. Piscanec, S. K. Saha, U. V. Waghmare, K. S. Novoselov, H. R. Krishnamurthy, A. K. Geim, A. C. Ferrari, A. K. Sood, *Nat. Nanotechnol.* **2008**, *3*, 210.
[40] R. Voggu, C. S. Rout, A. D. Franklin, T. S. Fisher, C. N. R. Rao, *J. Phys. Chem. C* **2008**, *112*, 13053.
[41] J. Barthel, L. Houben, K. Tillmann, *JLSRF* **2015**, *1*, A34.
[42] A. Kovács, R. Schierholz, K. Tillmann, *JLSRF* **2016**, *2*, A43.
[43] H. C. Du, *Ultramicroscopy* **2015**, *151*, 62.

Manuscript received: December 2, 2016
Final Article published: January 11, 2017

